Published in final edited form as:
Proteins. 2014 December ; 82(12): 3476–3482. doi:10.1002/prot.24702.

Crystal structure of human Ankyrin G death domain

Ying Liu[1], **Yan Zhang**[1,3], and **Jia-huai Wang**[1,2]

Ying Liu: lylucky@pku.edu.cn; Yan Zhang: yanzhang@pku.edu.cn; Jia-huai Wang: jwang@red.dfci.harvard.edu

[1]State Key Laboratory of Biomembrane and Membrane Biotechnology, College of Life Sciences, Peking University, Beijing, 100871, China

[2]Dana-Farber Cancer Institute, Harvard Medical School, Boston, MA. 02115, USA

[3]PKU-IDG/McGovern Institute for Brain Research, Beijing, 100871, China

Abstract

Ankyrins (Ank) are a ubiquitously expressed family of multifunctional membrane adapter proteins. Ankyrin G (AnkG) is critical for assembling and maintenance of the axon initial segment (AIS). Here we present the 2.1 Å crystal structure of human AnkG death domain (hAnkG-DD). The core death domain is composed of six α-helices and three 3_{10}-helices. It forms a hydrophobic pocket on the surface of the molecule. The C-terminal tail of the hAnkG-DD curves back to have the aromatic ring of a phenylalanine residue, Phe100 insert into this pocket, which anchors the flexible tail onto the core domain. Related DDs were selected for structure comparison. The major variations are at the C-terminal region, including the α6 and the long C-terminal extension. The results of size exclusion chromatography and analytical ultracentrifugation suggest that hAnkG-DD exists as monomer in solution. Our work should help for the future investigation of the structure-function of AnkG.

Keywords

apoptosis; axon initial segment; 3_{10}-helix; hydrophobic pocket; monomer

Introduction

Ankyrins are a ubiquitously expressed family of multifunctional membrane adapter proteins. The family members comprise three conserved domains as well as specialized domains found in alternatively spliced isoforms. The conserved domains include an N-terminal membrane-binding domain (MBD) composed of ANK repeats, a spectrin-binding domain (SBD), and a death domain (DD) located near the C-terminus [(1)]. Vertebrate Ank polypeptides fall into three classes: AnkR (R for restricted distribution, encoded by *Ank1*), AnkB (B for broadly expressed, encoded by *Ank2*), and AnkG (G for giant size and general expression, encoded by *Ank3*). Each class contains multiple alternatively spliced variants [(2)].

Corresponding author: Jiahuai Wang, State Key Laboratory of Biomembrane and Membrane Biotechnology, College of Life Sciences, Peking University, Beijing, 100871, China. Dana-Farber Cancer Institute, Harvard Medical School, Boston, MA. 02225, USA, jwang@red.dfci.harvard.edu.

AnkG plays an important role in neurons. Neurons are highly polarized cells in morphology and function with the dendrites that receive signals from other neurons and the axons that initiate and propagate action potential [3]. The initiation of action potential happens at a specialized structure located within the proximal axon of a neuron, named the axon initial segment (AIS) [3–5]. AnkG is critical for assembling and maintenance of the AIS [6–11]. Mice lacking AnkG also lack the AIS [8]. The cultured neurons with AnkG knocked down never develop the AIS [12].

AnkG binds, through MBD, to various membrane proteins, including ion channels (sodium channel [1, 8] and potassium channel [13]) and cell adhesion molecules (NrCAM [1] and neurofascin [12]). AnkG is also a cytoskeletal scaffold, associating with βIV spectrin through SBD [14]. It was reported that the DD of AnkG forms complexes with Fas and FADD, promoting Fas mediated apoptosis *in vitro* [15]. However, the structure and function of the DD of AnkG is unknown.

The Death domain was initially found in the cytoplasmic part of Fas antigen and type I tumor necrosis factor (TNF) receptor. This novel domain is required for apoptosis, hence the name of death domain [16]. The domain was soon to be found in a superfamily transducing a death signal. It actually plays a more general role (not just for “death”) as a module in mediating protein-protein interaction for diverse cellular functions in many systems [17]. Four DD subfamilies have been structurally defined [18].

We present here the 2.1 Å crystal structure of human AnkG death domain (hAnkG-DD). The core DD is composed of six α-helices and three 3_{10}-helices. It forms a hydrophobic pocket on the surface of the molecule. The C-terminal tail of the DD curves back to have the aromatic ring of a phenylalanine residue, Phe100 insert into this pocket, which anchors the flexible tail onto the core domain. Related DDs were selected for structure comparison. The major variations are at the C-terminal region, including the α6 and the long C-terminal extension. The results of size exclusion chromatography and analytical ultracentrifugation suggest that hAnkG-DD exists as monomer in solution. Our work should help for the future investigation of the structure-function of AnkG.

Methods

Cloning, expression, and purification of AnkG-DD

The DNA fragment of hAnkG-DD (residues 609–720, NP_001140.2) was amplified by PCR from cDNA library of human embryo. The DNA sequences of 5’-CTAATCATATGGAACGGACAGATATCAGGATGG-3’ and 5’-ATTTACTCGAGACCATCAACAGGGTCATGG-3’ were used as sense and anti-sense primer respectively. Five protection bases were included in each primer at the 5’ end. The amplified DNA fragment was double digested and inserted into pET21b at the position between NdeI and XhoI recognition sites. The DNA sequence of hAnkG-DD was verified by sequencing (Invitrogen) the construct. The confirmed hAnkG-DD-pET21b plasmid was transformed into E.coli strain BL21(DE3). The protein expression of hAnkG-DD was induced by 1mM IPTG after OD600 reached 0.8. The cells were harvested after six-hour induction at 37 °C. The target protein was purified from cell lysate by Ni column (Qiagen

Ni-NTA agarose) and dialyzed in 20mM Tris-HCl, pH8.0, 100mM NaCl. The purity of protein was monitored by SDS-PAGE (15% polyacrylamide gel). The protein concentration was measured by OD280 absorbance with NanoDrop 2000 (Thermo scientific).

Crystallization

The hAnkG-DD protein was concentrated to 20mg/ml after purification. The hanging drop vapor diffusion method was used for crystallization. The well solution contains 0.2 M Sodium acetate trihydrate, 0.1 M Tris hydrochloride pH 8.5, 30% w/v Polyethylene glycol 4,000. It was crystallized at 18 °C.

The crystals were optimized by seeding procedure. One single crystal was harvested into 50 μl stabilization buffer (well solution containing 20% glycerol). Seed Bead (Hampton Research HR2–320) was used to grind the crystal into invisible tiny weenie spots by vortex. It was followed by a serial dilution with the stabilization buffer. The ratio is 1 to 10. The seeding dilutions of 1:10, $1:10^2$, $1:10^3$, and $1: 10^4$ were used respectively for optimization. Each hanging drop of 2 μl volume contains 1μl seeding dilution and 1μl protein sample.

Data collection

X-ray diffraction data of hAnkG-DD were collected on Beamline BL17U1 at Shanghai Synchrotron Radiation Facility (SSRF). The detector of ADSC Quantum 315r CCD was used for data collection. The distance between the crystal and detector was 300 mm. The wavelength was adjusted to 0.98 Å. It was set up for 1 second as the exposure time, and 1 degree as the oscillation per frame. Altogether 270 frames were collected for the whole data set.

Structure determination and refinement

The raw data were indexed, integrated, and scaled with HKL2000 [19]. The structure was determined using molecular replacement with molrep [20, 21] in CCP4 [22] package. The DD of hAnkB has the highest sequence similarity with hAnkG-DD (63% identities and 79% positives) in the RCSB protein data bank. Therefore the truncated model of 4D8O (residue 1452–1529, hAnkB-DD) was selected as the search model for phasing. The structure went through rounds of alternate refinement and model re-building with Phenix [23] and Coot [24].

Analytical ultracentrifugation (AUC)

It was performed on the Beckman Optima XL-I analytical ultracentrifuge by sedimentation velocity method. The An-60 Ti rotor was used. The protein sample was diluted to three different concentrations (2.5 mg/ml, 3 mg/ml, 3.5 mg/ml) and loaded into the cell chamber (~300 μl) against buffer blank respectively. The wavelength was adjusted to 293 nm to make the absorbance around 1.0. It was centrifuged at 60,000 rpm for 7 hours. Sedimentation profiles were analyzed with the software SEDFIT.

Results

Structure of hAnkG-DD

It took 2 months for the crystals to appear in the first crystallization trial. However, by seeding, well-grown rod-like crystal cluster can be obtained within one week. These crystals are good enough for data collection.

The statistics of the data set and the structure refinement are shown in Table 1. The hAnkG-DD crystallizes in orthorhombic space group $P2_12_12_1$ with the unit cell parameters a=44.5 Å b=56.8 Å c=82.0 Å. There are two molecules in one asymmetric unit. The Matthew's coefficient is 1.87 calculated by CCP4 [22] (Matthews_coef [25, 26]), with the solvent content being 34.4%. The 2.1 Å structure was refined to R_{work} and R_{free} reaching 0.18 and 0.23 respectively. The Ramachandran plot of the structure is very good with 97.8% residues in the most favorable regions, 2.2% residues in the allowed regions, and none in disallowed regions. High-quality electron density map allowed for the tracing of both molecules from residues Glu2[a] to Ala101. Only residues Gly96 and Thr97 in molecule A and residues Asn93-Ser97 in molecule B do not have density for modeling. The structure has been deposited into RCSB protein data bank (PDB ID: 4O6X).

The crystal structure of hAnkG-DD is shown in Fig. 1A. It has the common DD fold, consisting six α-helices (α1–α6) antiparallel to one another. It also contains three 3_{10} helix (η1–η3, Fig. 1A red), which varies among DDs. η1 (residue 16–18) locates at the linker between α1 and α2, and the beginning of α2. η2 (residue 60–62) resides right after α4. η3 (residue 87–92) is on the C-terminal extension. The core domains of the two molecules (chain A and B) in the same asymmetric unit can be superimposed really well. Obvious deviations can only be seen at the C-terminal region (Fig. 1B). Both molecules have a C-terminal tail with the sequence Arg-Ser-Phe-Ala (residue 98–101) clearly defined by the electron density (Fig. 1C), whereas the residues 96–97 in both molecules are disordered. The reason for this "broken" tail to be well-placed is that the aromatic side chain of Phe100 on the tail pokes into the hydrophobic pocket formed by the core domain. The aliphatic side chains of residue Met8, Leu52, Val56, Leu68, Leu84, Ile94 contribute to the formation of the pocket (Fig. 1D, in red). The electrostatic surface of the model is displayed in Fig. 1E (chain A only), with (left) and without (right) the C-terminal tail. It shows that, besides Phe100, all of the other residues on the tail are inlaid well in the groove next to the hydrophobic pocket. They have specific interactions with the core domain. Interestingly, the two molecules in the same asymmetric unit do not utilize the exactly same way for the tail binding (Fig. 1B).

a. The residues are numbered on the basis of the experimental construct in this research. The initiating methionine is taken as residue 1. The E2 in construct equals to E609 in the full length hAnkG

Structure comparison of hAnkG-DD with related DDs

Among the available protein structures, hAnkG-DD has the highest sequence identity with the DDs of the other two Ank family members. It shares 63% identity with hAnkB-DD (4D8O), and 56% with hAnkR-DD (2YVI). It also has 34% identity with the DD of mouse

FADD (1FAD). The sequence alignment of the DD fragments mentioned above is shown in Fig. 2. The structure comparisons are depicted in Fig. 3. The conformation of C-terminal region varies the most among DDs. The C-terminal α6 of hAnkB-DD is very short, with only five residues. By contrast, hAnkG-DD has a α6 twice as long and also a lengthy C-terminal extension (Fig. 3A). The hAnkR-DD has a similar length of α6 with that of hAnkG-DD, but lacks the C-terminal extension (Fig. 3B). The FADD-DD has a longer α6 than that of hAnkG-DD, but no 3_{10} helix extension (Fig. 3C). It was reported that the Fas-DD and FADD-DD can be pulled down by AnkG-DD [(15)]. The FADD-DD shares similarities with AnkG-DD, while the protein sequence identities between Fas-DD and AnkG-DD is less than 20%. Therefore the comparison of hAnkG-DD and Fas-DD (1DDF) is included in Fig. 3D. The α6 of Fas-DD is much longer than that of hAnkG-DD. But the further C-terminal conformation is not available. The RMSD value between compared structures is given in table 2. The truncated 4D8O was used for phasing to determine the 4O6X. It may explain the low rmsd of 0.46 Å.

hAnkG-DD exists as homogeneous monomer in solution

The interfaces between chain A and B in crystal contacts were analyzed by PISA (v1.48) [(27)]. Two of them have more prominent buried area than the others. The interface 1 has the largest buried area of 616.0 $Å^2$ but very high energy level (−0.4 kcal/mol). Therefore it gets 0.0 in Complex Formation Significance Score (CSS). However, the interface 2 has a less buried area of 583.6 $Å^2$ with comparably low energy (−5.7 kcal/mol). It scores 0.1 in CSS. It implies that the interface 2 might play an auxiliary roll in dimer formation. Since these are still very small buried surface area, the size exclusion chromatography and analytical ultracentrifugation (AUC) were carried out for further investigation.

The profile of size exclusion chromatography (GE, HiLoad 16/60 Superdex 200) is depicted in Fig. 4A. It shows clean and sharp one peak only. The peak locates where the monomer is supposed to be, on the basis of a rough molecular weight estimate of global proteins. It suggests that the hAnkG-DD exists as homogeneous monomer in solution. The results of AUC further confirmed the monomeric state of hAnkG-DD in solution (Fig. 4B).

Discussion

The crystal structure of hAnkG-DD reveals a conserved six-helix bundle. A hydrophobic pocket locates at one end of the bundle, encompassed by α1 and α4–6 (Fig. 1A). Both Chain A and B have poor electron density at C-terminal extension between the core DD and the very C-terminus. Those residues that can be built in the region assume different conformations between chain A and B (Fig. 1B). It suggests that this part of the molecule is flexible. However, a four-residue tail in this region is stabilized to a certain extent by the anchoring of Phe100 sidechain into the hydrophobic pocket. Despite of that, the conformation of the tail varies from A to B (Fig. 1B). It is unknown whether the Phe100 insertion into the hydrophobic pocket is of any biological significance. The hypothesis is that the four-residue tail may act as an inhibiter to cover the active site of the hydrophobic pocket. If so, it is reasonable that the tail is not fully constrained.

The deviations of the DD C-terminal regions in 3D structures come from the variations in the protein sequences. Basically, there is not a single consensus residue outside the core DD (from E85 to the C-terminal end) among the four aligned sequences (Fig. 2). It may be related to their diversified functions. One interesting feature of our 4O6X structure is that its N-terminal α1 tilts more outwards compared with other structures. It is likely due to the push from the Phe100 insertion (compared to 4D8O for instance, Fig. S1). Furthermore, the 4O6X-α6 inclines more inwards for a tight molecular packing. It seems possible that the Phe100 insertion somehow changes the conformation of the intact core DD. In terms of electrostatic surface, no conspicuous hydrophobic pocket is found on the model of 4D8O and 2YVI, while it looks like a hydrophobic hole at the corresponding site of 1FAD. But it is a proline in 1FAD at the same position as 4O6X-Phe100 (Fig. 2). It does not seem to be inserted into the hole. Besides, there is no aromatic residue for the hole on the entire C-terminal region of 1FAD. A tyrosine locates at the 4O6X-Phe100 position in 4D8O. It is most possible that the hAnkB-DD will have a closer conformation to hAnkG-DD, if the C-terminal region is added. It hypothesized that with the side chain of tyrosine insertion, the hydrophobic pocket will be opened. In RCSB protein data bank, most DD structures lack the information of C-terminal region conformation. The 4O6X model may shed light on the functional importance of this region after the core DDs. To prove that, it is awaiting the new binding partners of hAnkG-DD to be discovered. It was reported that the Fas-DD and FADD DD can be pulled down by AnkG-DD [(15)].

But the binding mode is not clear yet. FADD-DD interacts with Fas-DD and changed the conformation of Fas-DD. The protein sequence of hAnkG-DD shares the highest identity and similarity with FADD-DD out of the Ank family. It is possible that AnkG-DD binds to Fas-DD similar as FADD-DD. It is also possible that AnkG-DD binds to other DDs through its long C-terminal tail, in a similar manner like how *Drosophila melanogaster* Tube-DD binds to Pelle-DD [(28)]. If so, the C-terminal tail of hAnkG-DD would have to undock from the core domain in order to bind other DD partners (Fig. S2). Both hAnkG-DD and dTube-DD have a ‘PVDF’ motif on the C-terminal tail, which is very close to the Pelle-DD binding site on the dTube-DD. More biochemical data is needed to make the deduction.

Supplementary Material

Refer to Web version on PubMed Central for supplementary material.

Acknowledgements

We appreciate prof. Junyu Xiao for computational help. We thank Dr. Zhaoyang Ye for technical help. We thank prof. Yunyu Shi, Dr. Fudong Li, and Dr. Zhonghua Liu for sharing their beam time at Shanghai Synchrotron Radiation Facility (SSRF). We also thank all the staffs at SSRF for their support. The work was funded by the Ministry of Education of China to J.-H.W. and Y.Z., the National Science Foundation of China (NSFC) Major Research Grant (91132718) and the Beijing Natural Science Foundation (7142085) to Y.Z., an NIH grant (HL48675) and funds from the Peking-Tsinghua Center for Life Sciences to J-H W.

References

1. Bennett V, Chen L. Ankyrins and cellular targeting of diverse membrane proteins to physiological sites. Curr Opin Cell Biol. 2001; 13:61–67. [PubMed: 11163135]

2. Mohler PJ, Gramolini AO, Bennett V. Ankyrins. J Cell Sci. 2002; 115:1565–1566. [PubMed: 11950874]
3. Rasband MN. The axon initial segment and the maintenance of neuronal polarity. Nat Rev Neurosci. 2010; 11:552–562. [PubMed: 20631711]
4. Palay SL, Sotelo C, Peters A, Orkand PM. The axon hillock and the initial segment. J Cell Biol. 1968; 38:193–201. [PubMed: 5691973]
5. Buffington SA, Rasband MN. The axon initial segment in nervous system disease and injury. Eur J Neurosci. 2011; 34:1609–1619. [PubMed: 22103418]
6. Kapfhamer D, Miller DE, Lambert S, Bennett V, Glover TW, Burmeister M. Chromosomal localization of the ankyrinG gene (ANK3/Ank3) to human 10q21 and mouse 10. Genomics. 1995; 27:189–191. [PubMed: 7665168]
7. Kordeli E, Lambert S, Bennett V. AnkyrinG. A new ankyrin gene with neural-specific isoforms localized at the axonal initial segment and node of Ranvier. J Biol Chem. 1995; 270:2352–2359. [PubMed: 7836469]
8. Zhou D, Lambert S, Malen PL, Carpenter S, Boland LM, Bennett V. AnkyrinG is required for clustering of voltage-gated Na channels at axon initial segments and for normal action potential firing. J Cell Biol. 1998; 143:1295–1304. [PubMed: 9832557]
9. Hedstrom KL, Ogawa Y, Rasband MN. AnkyrinG is required for maintenance of the axon initial segment and neuronal polarity. J Cell Biol. 2008; 183:635–640. [PubMed: 19001126]
10. Sobotzik JM, Sie JM, Politi C, Del Turco D, Bennett V, Deller T, Schultz C. AnkyrinG is required to maintain axo-dendritic polarity in vivo. Proc Natl Acad Sci U S A. 2009; 106:17564–17569. [PubMed: 19805144]
11. Szu-Yu Ho T, Rasband MN. Maintenance of neuronal polarity. Dev Neurobiol. 2011; 71:474–482. [PubMed: 21557501]
12. Hedstrom KL, Xu X, Ogawa Y, Frischknecht R, Seidenbecher CI, Shrager P, Rasband MN. Neurofascin assembles a specialized extracellular matrix at the axon initial segment. J Cell Biol. 2007; 178:875–886. [PubMed: 17709431]
13. San-Cristobal P, Lainez S, Dimke H, de Graaf MJ, Hoenderop JG, Bindels RJ. Ankyrin-3 is a novel binding partner of the voltage-gated potassium channel Kv1.1 implicated in renal magnesium handling. Kidney Int. 2014; 85:94–102. [PubMed: 23903368]
14. Yang Y, Ogawa Y, Hedstrom KL, Rasband MN. betaIV spectrin is recruited to axon initial segments and nodes of Ranvier by ankyrinG. J Cell Biol. 2007; 176:509–519. [PubMed: 17283186]
15. Del Rio M, Imam A, DeLeon M, Gomez G, Mishra J, Ma Q, Parikh S, Devarajan P. The death domain of kidney ankyrin interacts with Fas and promotes Fas-mediated cell death in renal epithelia. J Am Soc Nephrol. 2004; 15:41–51. [PubMed: 14694156]
16. Itoh N, Nagata S. A novel protein domain required for apoptosis. Mutational analysis of human Fas antigen. J Biol Chem. 1993; 268:10932–10937. [PubMed: 7684370]
17. Feinstein E, Kimchi A, Wallach D, Boldin M, Varfolomeev E. The death domain: a module shared by proteins with diverse cellular functions. Trends Biochem Sci. 1995; 20:342–344. [PubMed: 7482697]
18. Park HH, Lo YC, Lin SC, Wang L, Yang JK, Wu H. The death domain superfamily in intracellular signaling of apoptosis and inflammation. Annu Rev Immunol. 2007; 25:561–586. [PubMed: 17201679]
19. Z Otwinowski WM. Processing of X-ray Diffraction Data Collected in Oscillation Mode. Methods in Enzymology: Macromolecular Crystallography, part A. 1997; 276:307–326.
20. Vagin AA. New translation and packing functions. Newsletter on protein crystallography, Daresbury Laboratory. 1989; 24:117–121.
21. A Vagin AT. MOLREP: an automated program for molecular replacement. J. Appl. Cryst. 1997; 30:1022–1025.
22. Collaborative Computational Project, N. The CCP4 suite: programs for protein crystallography. Acta Crystallogr D Biol Crystallogr. 1994; 50:760–763. [PubMed: 15299374]
23. Adams PD, Afonine PV, Bunkoczi G, Chen VB, Davis IW, Echols N, Headd JJ, Hung LW, Kapral GJ, Grosse-Kunstleve RW, McCoy AJ, Moriarty NW, Oeffner R, Read RJ, Richardson DC,

Richardson JS, Terwilliger TC, Zwart PH. PHENIX: a comprehensive Python-based system for macromolecular structure solution. Acta Crystallogr D Biol Crystallogr. 2010; 66:213–221. [PubMed: 20124702]

24. Emsley P, Lohkamp B, Scott WG, Cowtan K. Features and development of Coot. Acta Crystallogr D Biol Crystallogr. 2010; 66:486–501. [PubMed: 20383002]
25. Matthews BW. Solvent content of protein crystals. J Mol Biol. 1968; 33:491–497. [PubMed: 5700707]
26. Kantardjieff KA, Rupp B. Matthews coefficient probabilities: Improved estimates for unit cell contents of proteins, DNA, protein-nucleic acid complex crystals. Protein Sci. 2003; 12:1865–1871. [PubMed: 12930986]
27. Krissinel E, Henrick K. Inference of macromolecular assemblies from crystalline state. J Mol Biol. 2007; 372:774–797. [PubMed: 17681537]
28. Xiao T, Towb P, Wasserman SA, Sprang SR. Three-dimensional structure of a complex between the death domains of Pelle and Tube. Cell. 1999; 99:545–555. [PubMed: 10589682]

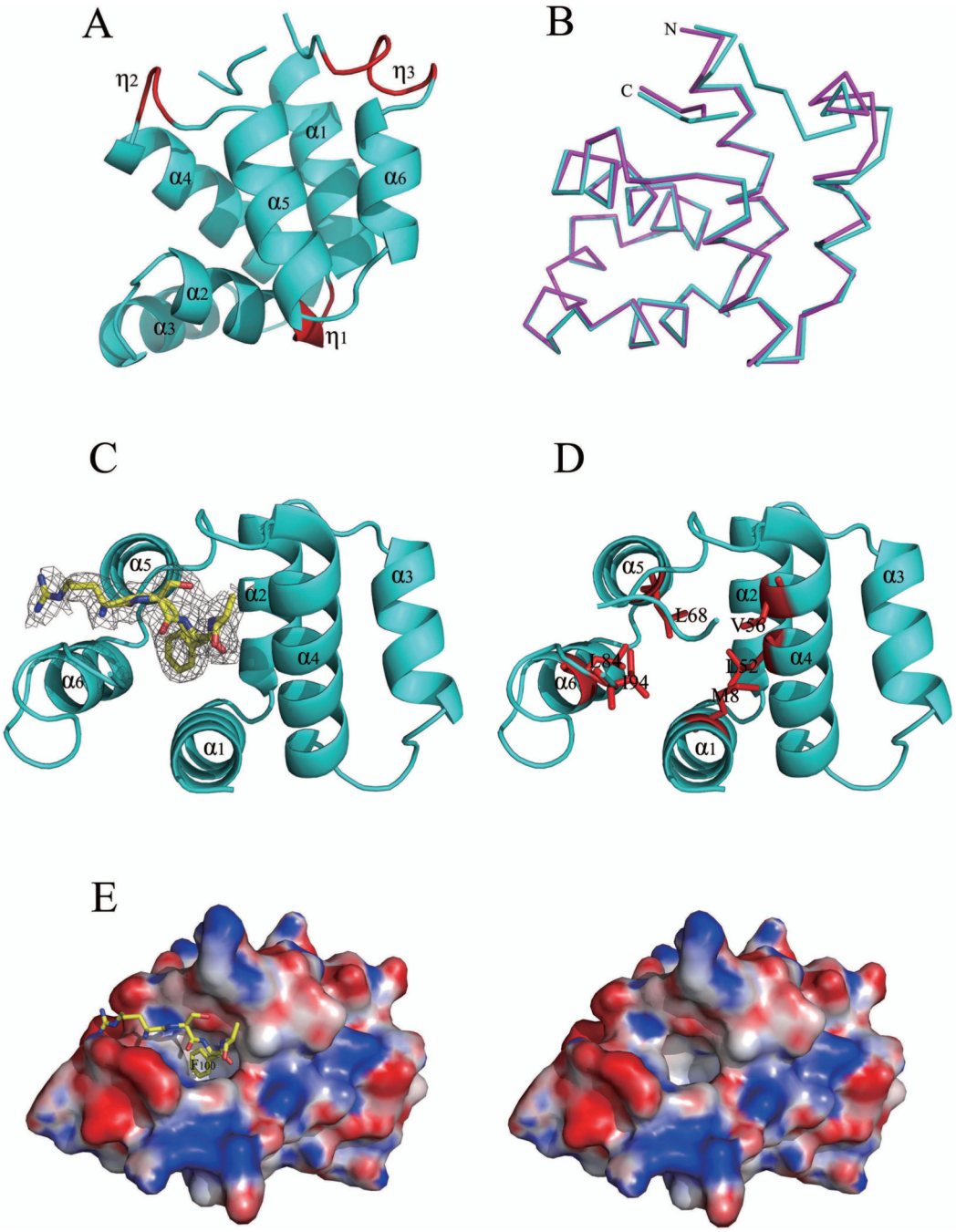

Figure 1.

Crystal structure of hAnkG-DD. A. Ribbon representation of chain A. The secondary structure elements are highlighted. The 3_{10} helixes are colored red. B. Backbone superposition of chain A (cyan) and B (magenta). The N- and C- termini are labeled. C. Electron density map of the C-terminal tail. The four-residue C-terminal tail is shown by sticks, with the electron density map in grey grid. Other region of the molecule is depicted with cyan ribbon. D. Residues involved in the formation of the hydrophobic pocket (highlighted in red). E. Electrostatic surface of the hydrophobic pocket with (left) and

without (right) the C-terminal tail. The red is for negative potential, blue for positive, and white for hydrophobic.

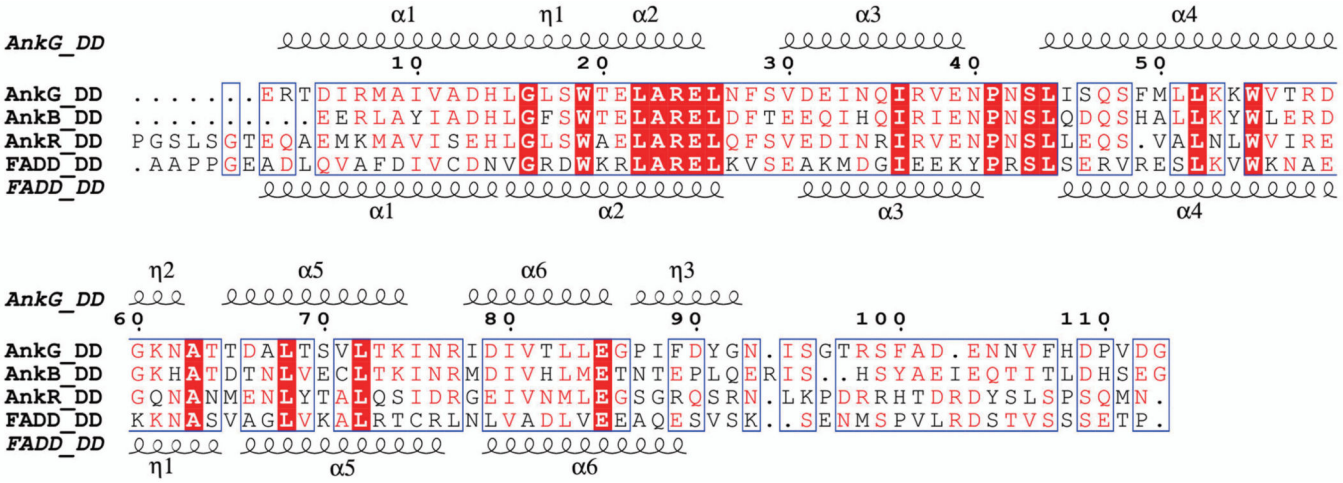

Figure 2.

Sequence alignment of related DDs. Residues identical in all sequences are highlighted in red columns. Conserved residues are colored red in blue columns. The secondary structure elements of AnkG-DD are shown on the top. Those of FADD-DD are drawn at the bottom.

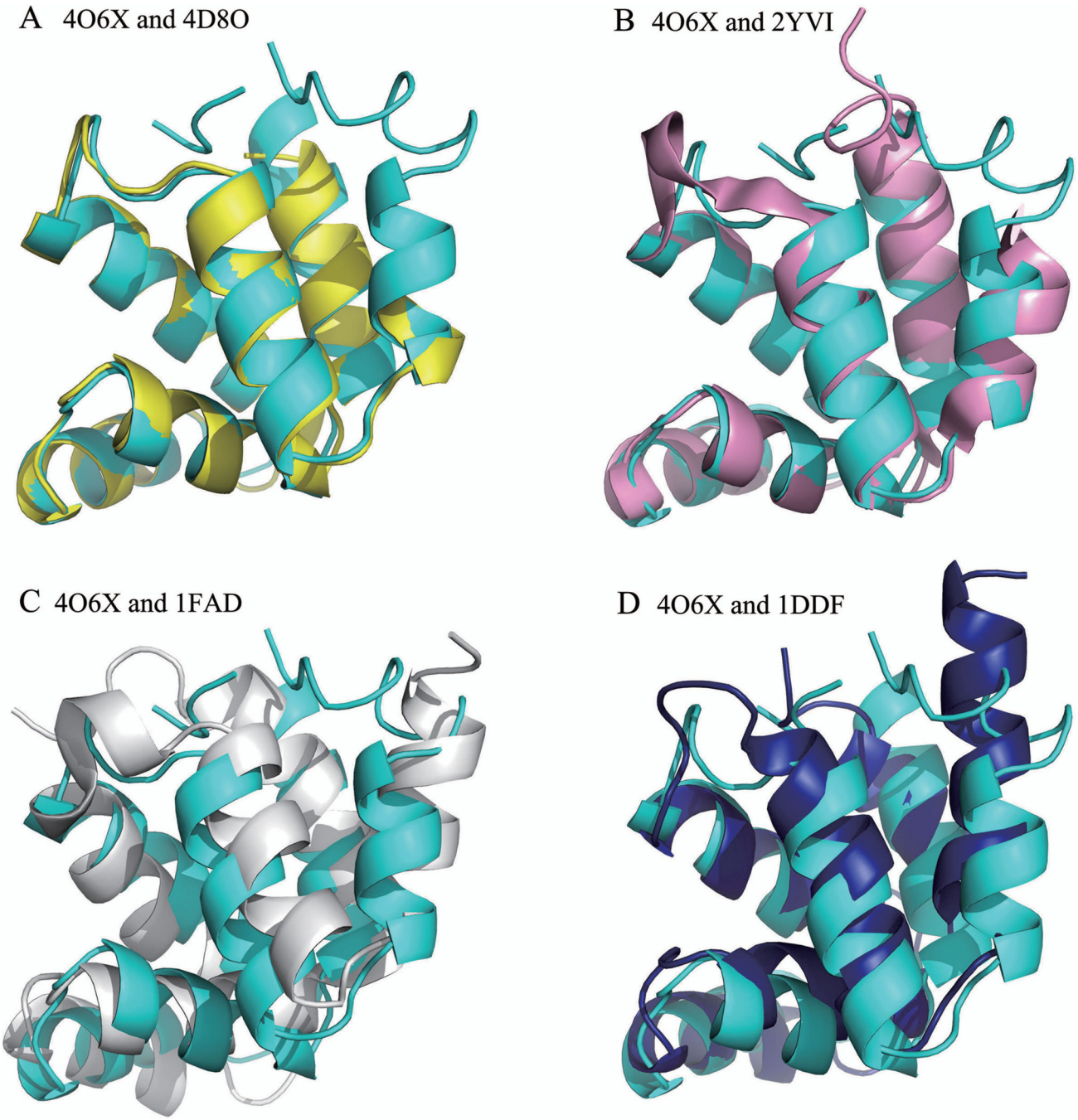

Figure 3.

Backbone superposition of hAnkG-DD with related DDs. A. 4O6X (hAnkG-DD, cyan) and 4D8O (hAnkB-DD, yellow). B. 4O6X (hAnkG-DD, cyan) and 2YVI (hAnkR-DD, pink). C. 4O6X (hAnkG-DD, cyan) and 1FAD (mFADD, white). D. 4O6X (hAnkG-DD, cyan) and 1DDF (hFas-DD, blue).

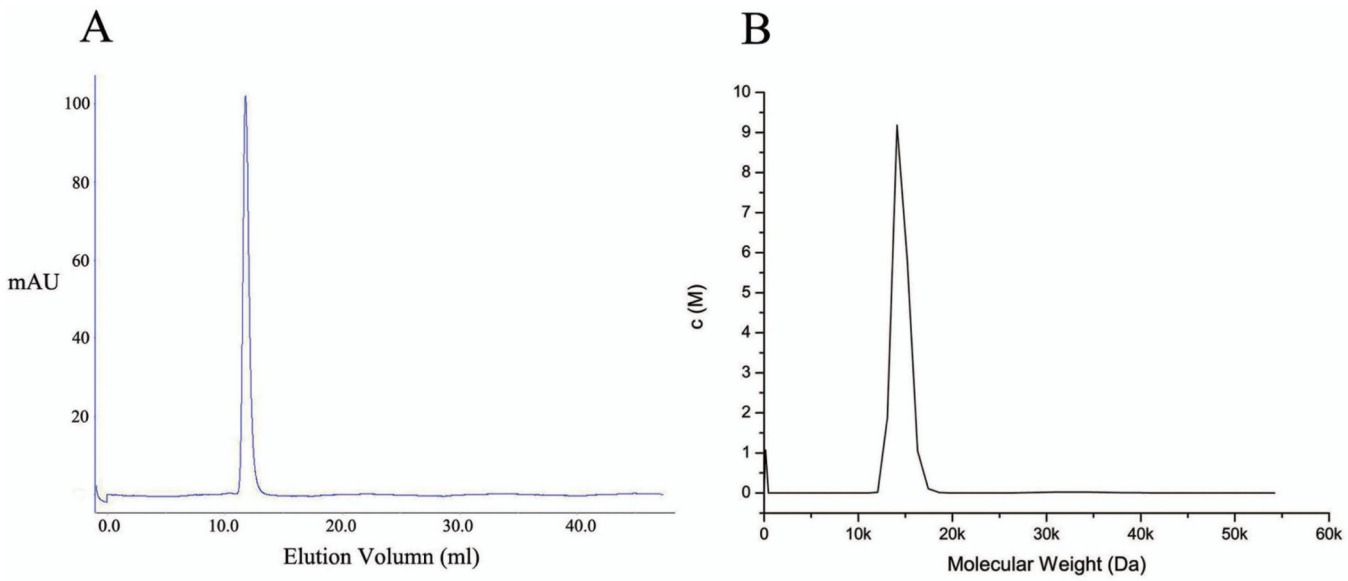

Figure 4.

The DD of hAnkG exists as homogeneous monomers in solution. A. The profile of UV (λ280) absorbance generated from size exclusion chromatography (GE, HiLoad 16/60 Superdex 200). B. The profile of sedimentation coefficients against molecular weight generated from AUC at λ_{293}.

Table 1

Statistics of data collection and refinement

Data		AnkyrinG death domain
Data collection		
Integration Package		HKL2000
Wavelength (Å)		0.9798
Space group		$P2_12_12_1$
Unit Cell:	a, b, c (Å)	44.45, 56.82, 81.95
	α, β, γ (°)	90.0, 90.0, 90.0
Resolution (Å)		50-2.10 (2.14-2.10)
R_{merge} (%)[b]		7.5 (67.3)
Mean **I**/sigma(**I**)		25.7 (3.0)
Completeness (%)		99.1 (99.5)
Number of measured reflections		98,856 (4,811)
Number of unique reflections		12,488 (594)
Redundancy		7.9 (8.1)
Molecules in an asymmetric unit		2
Structure Refinement		
Resolution range (Å)		39.08-2.10 (2.31-2.10)
No. reflections (work/free)		11,928/587 (2,570/133)
R_{work} (%)[c]		18.2
R_{free} (%)		23.1
No. atoms		
Protein		1540
Water		66
Average B-factors (Å^2)		
Overall		48.7
Protein		48.8
Water		46.7
R.m.s deviations from ideal values		
Bond lengths (Å)		0.006
Bond angles (°)		0.90
Ramachandran plot statistics (%)		
Most favorable		97.8
Allowed		2.2
Disallowed		0

[a] Values of the highest resolution shell are shown in parentheses.

[b] $R_{merge}=\Sigma h\Sigma i|Ih,i-Ih|/\Sigma h\Sigma i Ih,i$, where *Ih* is the mean intensity of the *i* observations of symmetry related reflections of *h*.

[c] $R_{work} = \Sigma|Fobs-Fcalc|/\Sigma Fobs$, where *Fcalc* is the calculated protein structure factor from the atomic model (R_{free} was calculated with 5% of the reflections selected).

Table 2

RMSD values of compared structures

Structure 1 (residue 2–101)	Structure 2	Compared residues of structure 2	RMSD value (Å)
4O6X	4D8O	residue 1452–1529	0.47
4O6X	2YVI	residue 1394–1497	0.85
4O6X	1FAD	residue 89–183	2.63
4O6X	1DDF	residue 212–303	2.81